Article

SYNTHESIS, BIOCHEMICAL AND *IN SILICO* EXPLORATION OF NOVEL IMIDAZOLE BASED 1,2,3-TRIAZOLES AS POTENTIAL HIT AGAINST CARBONIC ANHYDRASE II ISOZYME

Mumtaz Hussain[a], Pervaiz Ali Channar[b,*], Aisha A. Alsfouk[c], Syeda Abida Ejaz[d,*], Mubashir Aziz[d], Zahid Hussain[a], Ghulam Abbas Kandhro[b], Hafiz Muhammad Attaullah[d], Rabail Ujhan[e], Mushtaque Ali Jakhrani[f], Aamer Saeed[g,*], Qamar Abbas[h,i] and Laith Abualigah[j,k,l,m]

[a]Department of Chemistry, University of Karachi, 75270 Karachi, Pakistan
[b]Department of Basic Sciences and Humanities, Faculty of Information Science and Humanities, Dawood University of Engineering and Technology, 74800 Karachi, Pakistan
[c]Department of Pharmaceutical Sciences, College of Pharmacy, Princess Nourah Bint Abdulrahman University, P.O. Box 84428, 11671 Riyadh, Saudi Arabia
[d]Department of Pharmaceutical Chemistry, Faculty of Pharmacy, The Islamia University of Bahawalpur, 63100 Bahawalpur, Pakistan
[e]Dr. M. A. Kazi Institute of Chemistry, University of Sindh, 76080 Jamshoro, Pakistan
[f]Institute of Chemistry, Shah Abdul Latif University, 66020 Khairpur, Pakistan
[g]Department of Chemistry, Quaid-I-Azam University, 45320 Islamabad, Pakistan
[h]Department of Biology, College of Science, University of Bahrain, 32038 Sakhir, Kingdom of Bahrain
[i]Department of Biological Sciences, College of Natural Sciences, Kongju National University, 32588 Gongju, Republic of Korea
[j]Hourani Center for Applied Scientific Research, Al-Ahliyya Amman University, 19328 Amman, Jordan
[k]MEU Research Unit, Middle East University, 11831 Amman, Jordan
[l]Department of Electrical and Computer Engineering, Lebanese American University, 135053 Byblos, Lebanon
[m]Applied Science Research Center, Applied Science Private University, 11931 Amman, Jordan

Received: 09/05/2023; accepted: 01/08/2024; published online: 03/13/2024

This study aimed to synthesize novel compounds as more effective carbonic anhydrase II inhibitors. For this purpose, 2-(3-methoxy-4-(prop-2-yn-1-yloxy)phenyl)-4,5-diphenyl-1*H*-imidazole (**3**) was reacted with 3-methoxy-4-(prop-2-yn-1-yloxy)benzaldehyde through the glyoxal reaction to produce a series of imidazole-based 1,2,3-triazoles **5a**-**f**. The synthesized compounds were structurally confirmed using IR, ^{1}H, and ^{13}C NMR techniques. To evaluate their potential as inhibitors of carbonic anhydrase II enzyme, the synthesized compounds were tested via *in vitro* enzyme inhibition assay. Among the derivatives, compounds **5f** and **5a** exhibited the most promising inhibitory potential, with IC_{50} values of 0.025 ± 0.001 and 0.032 ± 0.003 μM, respectively. Both **5a** and **5f** derivatives have comparable inhibitory potential but **5f** was found to be more potent than **5a**. Molecular docking analysis revealed that compounds **5a** and **5f** displayed excellent binding scores of −8.0 and −8.4 kcal mol^{-1}, respectively. The results were further validated by MD simulations. The RMSD analysis revealed the average values of 3.20 Å for the ligand-protein complex, 1.38 Å for the apoprotein, and 7.15 Å for the ligand molecule. Based on the chemical stability and biological importance, the compound **5f** was identified as potential lead candidates for the development of more effective carbonic anhydrase II inhibitors.

Keywords: synthesis; imidazole-based 1,2,3-triazoles; carbonic anhydrase II; molecular docking; DFT.

INTRODUCTION

Carbonic anhydrase II (CA II) is a zinc-containing enzyme that catalyzes various biochemical reactions.[1] It is one of the most extensively studied and widely distributed isozymes of carbonic anhydrase, found in various tissues and organs such as red blood cells, lungs, kidneys, and salivary glands. CA II is essential for maintaining acid-base balance and pH homeostasis in the body.[2] It is concerned with various physiological processes, including kidney function, respiration, and bone remodeling. In the lungs, CA II catalyzes the hydration of carbon dioxide to bicarbonate, which helps to regulate the pH of the blood. In the kidneys, CA II plays a critical role in the reabsorption of bicarbonate ions, which helps to regulate the pH of the urine.[3,4] Mutations in the CA II gene are associated with various diseases such as osteoporosis, renal tubular acidosis, and cerebral calcification.[5] In addition, CA II is also concerned with the progression of certain cancers, including breast, ovarian, and prostate cancer. Due to its critical role in several pathological and physiological processes, CA II is a target for various drugs and inhibitors as shown in Figure 1.[6-8] These inhibitors have been used to treat disorders such as glaucoma, epilepsy, and osteoporosis. CA II inhibition has also been investigated as a potential treatment strategy for certain cancers.[9,10]

Among different types of heterocyclic compounds, the 1*H*-1,2,3-triazole and imidazole groups are important in medicinal chemistry, agrochemicals, and pharmaceuticals.[11,12] Over the past few decades, there has been a significant increase in the number of compounds containing these groups. Imidazole compounds have demonstrated considerable potential in several scientific disciplines, including biology and pharmacology.[13] Many imidazole derivatives have been found to exhibit important biological properties, including anti-inflammatory, analgesic, antitubercular, anticancer, and antifungal effects.[14,15] Imidazole derivatives have also been found to be potent inhibitors of CA II. The imidazole scaffold has shown a leading potential in the discovery of effective CA II inhibitors due to its capacity to act as both a hydrogen bond donor and acceptor. Among the already reported CA II inhibitors, the 1,2,4-triazole-imidazole hybrid is one of the most effective CA II inhibitors, with an IC_{50}

*e-mail: abida.ejaz@iub.edu.pk; aamersaeed@yahoo.com; pervaiz.ali@duet.edu.pk

value of 5.5 nM.[16] Some imidazole-1-sulfonyl hydrazones and their derivatives have demonstrated low nanomolar potency in inhibiting CA II activity (Figure 1). Briefly, both the 1*H*-1,2,3-triazole and imidazole groups are important due to their numerous uses in the fields of biomedical, biochemical, material sciences, and pharmaceuticals.[17]

The synthesis of hybrids may be of particular interest to synthetic chemists due to their biological, medicinal, and industrial uses. As a result, the current study has focused on the synthesis of 1*H*-1,2,3-triazole-imidazole-based moieties by the well-established method of copper-catalyzed azide-alkyne cycloaddition (CuAAC).[18,19] Furthermore, the current investigation sheds light on the inhibitory capability of these derivatives against CA II as well as the chemical reactivity of novel imidazole and 1,2,3-triazole heterocyclic compounds. These findings could pave the way for the creation of novel CA II inhibitors.

EXPERIMENTAL

Chemistry

Thin layer chromatography (TLC) was employed to separate and visualize the distinct chemicals in a mixture by utilizing Merck Silica gel plates that were pre-coated with aluminium. The Rf-values of the final products were determined through this process. The melting point of the compounds was measured in open capillaries using a Gallenkamp melting point instrument (MP-D). Attenuated total reflection (ATR) based Shimadzu FTIR equipment (4000-400 cm^{-1}) were used to collect infrared spectra.[20] ^{1}H-NMR spectra in $CDCl_3$ solutions were acquired using a Bruker NMR 300 MHz spectrometer with TMS as an internal reference. NMR spectroscopy is a technique that uses magnetic characteristics of atomic nuclei to identify and analyze the structure and dynamics of molecules.[21] The chemical shift (δ) was given in ppm and the *J* values in Hz. Chemical shift describes the magnetic surroundings of a nucleus in a molecule, whereas *J* values describe the connection between two nearby nuclei. Lastly, ^{13}C-NMR spectra in deuterated solutions were obtained using a (75 MHz) NMR spectrometer. Carbon-13 NMR spectroscopy is a technique that uses the magnetic characteristics of carbon-13 nuclei to identify and describe carbon atoms in a molecule.[22] High-resolution mass spectrometry (HRMS) is an analytical technique that is used to determine the exact molecular masses of compounds present in a sample and here analysis was done by using time of flight (TOF) mass analyzer.[23] FTIR, ^{1}H-NMR and ^{13}C-NMR spectra of characterized compounds are given in Figures 1S-12S (Supplementary Material).

General experimental procedure for the synthesis of 1,4-disubstituted 1,2,3-triazoles 5a-f

By employing synthetic methods that ensured a brief reaction time, mild conditions, and high yields, a diverse range of novel 1,4-disubstituted 1,2,3-triazoles **5a-f** were successfully synthesized according to the previously reported method.[18]

To synthesize the target compounds **5a-f**, shown in Scheme 1, the first step was to mix glacial acetic acid solvent with glyoxal (0.47 mmol), 3-methoxy-4-(prop-2-yn-1-yloxy) benzaldehyde (0.71 mmol), and ammonium ion (3.76 mmol). After that, the reaction mixture was subjected to reflux for a total of 3 h. After the completion of the reaction, the mixture was poured into 300 mL of cold water, and dropwise additions of ammonium hydroxide were made to raise the pH level to 7.0. The resulting precipitates, which were pale yellow, were collected and then washed in ice water to get pure 2-(3-methoxy-4-(prop-2-yn-1-yloxy)phenyl)-4,5-diphenyl-1*H*-imidazole (**3**).

In the second step, 2-(3-methoxy-4-(prop-2-yn-1-yloxy)phenyl)-4,5-diphenyl-1*H*-imidazole (**3**) (1.0 g, 5.3 mmol), 20 mL of DMF and appropriate amount of 1-(3 azidopropoxy)aryl (**4a**-**4f**) (10.6 mmol, 2 equiv) were added to a 100 mL round-bottomed flask. Once a clear solution was obtained, 5 mol% of copper(II) sulfate pentahydrate (0.05 equiv) and 20 mol% of sodium ascorbate (0.2 equiv) were added under constant stirring at 100 °C for 18-24 h. The TLC with the solvent system EtOAc:*n*-hexane, was used to analyze the progress of the reaction as it proceeded on. After the completion of the reaction, the green color of the mixture changed to brown. After that, the reaction mixture was mixed in cold water, resulting in the formation of precipitates that were subsequently filtered and dried. To purify the products **5a-f**, silica gel column chromatography was employed using a 3:7 ratio of ethyl acetate to *n*-hexane as the eluent. Moreover, the individual synthesis and characterization data for each compound is given in the supplementary material.

Density functional theory (DFT) calculations

This study aimed to analyze the distribution of electrons around molecular geometry and the reactivity profile of compounds using density functional theory (DFT) calculations. Here, calculations of newly synthesized derivatives were carried out using the Guassian09 program[24] using Becke-3-parameter-Lee-Yang-Parr (B3LYP) in the 3-21G basis set.[25] Various global parameters were calculated as discussed in our previously published article.[26-28]

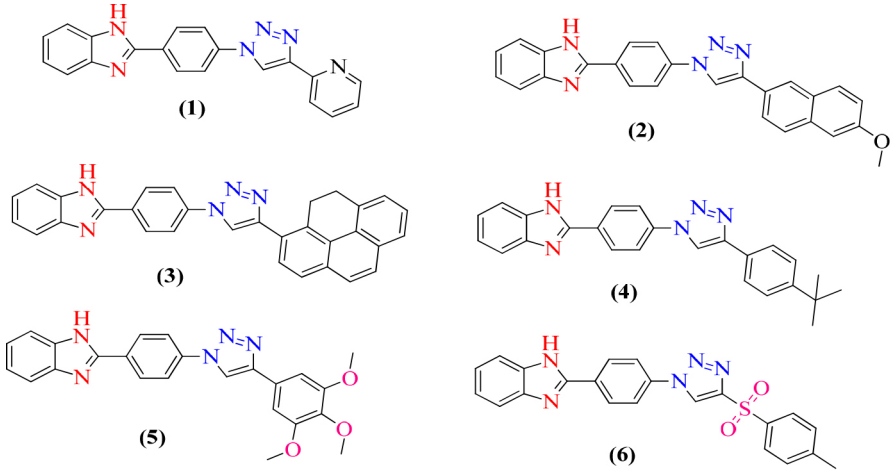

Figure 1. *Imidazole derivatives have reported biological activity against various targets*[6-8]

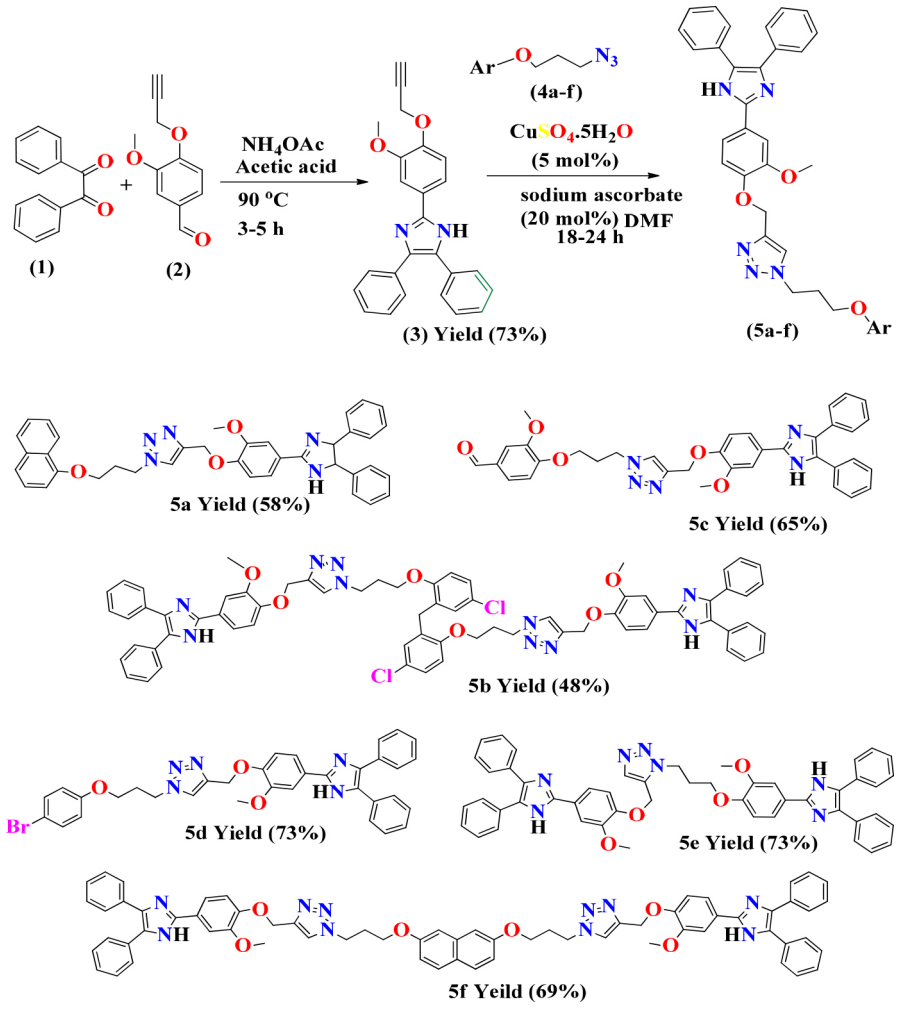

Scheme 1. *The synthesis scheme of 1,4-disubstituted 1,2,3-triazoles (**5a-f**)*

Carbonic anhydrase II assay

To determine the inhibition potential of the newly synthesized compounds **5a-f**, an analysis was conducted to assess their ability to inhibit carbonic anhydrase II. The study was carried out by using the previously reported method,[29,30] in which the assay was performed in 96 well plates. Initially, the 20.0 µL of compounds (1 mM) and 20.0 µL of CA II (50U) were mixed in 120.0 µL (50.0 mM) tris-sulfate buffer (pH 7.6). After 10 min of incubation, the substrate (*p*-nitrophenyl acetate) was added at the final concentration of 0.6 mM (40 µL) and the reaction mixture was again incubated for 20 min at 25 °C. The optical density was observed at 348 nm using a microplate reader (SpectraMax ABS, USA 96-well microplate reader). The percentage inhibition values and IC_{50} values were calculated using GraphPad Prism 5.0, as discussed earlier.[29]

Molecular docking

Molecular docking analysis on recently synthesized imidazole-based 1,2,3-triazoles was carried out to better understand the binding relationship between CA II and 1,2,3-triazoles derivatives along with acetazolamide as reference. The study was carried out using the 3D crystal structure of bovine carbonic anhydrase II, retrieved from Protein Data Bank (www.rcsb.com, PDB ID: 1V9E) with a resolution of 1.95 Å.[31,32] Before docking analysis, the targeted protein structure was prepared by using MGL tools. Heteroatoms and water molecules were removed, polar hydrogen and Kollman charges were added and structure was rendered for missing amino acid residues.[33] The energy-minimized 3D structures of all synthesized derivatives, **5a-f**, were drawn by using ChemDraw 3D.[34] All the compounds **5a-f** and reference compound acetazolamide were docked within an active pocket of CA II, using AutoDock's default genetic algorithm as the scoring function.[35] The dimensions of the grid box were set as (x: –18.045416, y: 30.891538; z: 19.161696). About 100 different configurations of docking complexes were generated for compounds **5a-f** and acetazolamide. Finally, the most stable configuration was selected for further analysis and development of 2D and 3D models.

Molecular dynamic simulation

Molecular dynamic (MD) simulations were used to observe the dynamic behavior and motion of atoms in a molecule over time.[36,37] In the current research, the visual molecular dynamics (VMD) interface was used to visualize the simulation trajectories and to predict the mechanical nature of the ligand, apoprotein, and ligand-protein complex. Initially, the ligand **5f** complex with CA II protein possessing the best binding energy was selected for MD simulations. A virtual environment was created by using the CHARMM36 (https://www.charmm-gui.org) force field to prepare topology files for MD simulations.[38] The system was solvated with a water box (TIP3P) under periodic boundary conditions and the pH of the system was maintained by the addition of Na and Cl ions (0.15 M). Finally, the system was equilibrated in NVT and NPT ensembles with Berendson thermostat and barostat at 300 k. The MD simulations were run

for 100 ns and output files were analyzed for structural stability of molecules under given conditions.[39,40]

ADMET analysis

The physicochemical and pharmacokinetic attributes of the synthesized derivatives were ascertained through ADMET predictor (Medchem designer 12.0). This computational tool facilitated a comprehensive assessment of several pharmacokinetic parameters, notably logP and logD, hydrogen bonding descriptors, polar surface area (PSA) and human intestinal absorption.[41]

RESULTS AND DISCUSSION

Chemistry

The synthesis of 1,4-disubstituted 1,2,3-triazoles **5a**-**f** was carried out by using 3-methoxy-4-(prop-2-yn-1-yloxy) benzaldehyde (0.71 mmol), glacial acetic acid solvent with glyoxal (0.47 mmol), and ammonium ion (3.76 mmol). The reaction mixture was then refluxed for 3 h. Once the reaction was completed, the mixture was poured into 300 mL of cold water and ammonium hydroxide was added dropwise to adjust the pH to 7. The resulting light-yellow precipitate was collected and washed with cold water. The crude product was obtained (**3**). In the second step methoxy-4-(prop-2-yn-1-yloxy)phenyl)-4,5-diphenyl-1*H*-imidazole (**3**) (1.0 g, 5.3 mmol), in 20 mL of DMF, and an appropriate amount of 1-(3 azidopropoxy)aryl **4a**-**f** (10.6 mmol, 2 equiv) were added to a 100 mL round-bottomed flask. Once a clear solution was obtained, 5 mol% of copper(II) sulfate pentahydrate (0.05 equiv) and 20 mol% of sodium ascorbate (0.2 equiv) were added under constant stirring. The reaction mixture was heated at 100 °C for 18-24 h and monitored by TLC using EtOAc:*n*-Hexane as the solvent system. The completion of the reaction was indicated by a color change from green to brown. The reaction mixture was then subjected to workup with cold water, and the resulting precipitates were filtered and dried. The products (**5a**-**f**) were further purified by silica gel column chromatography using ethyl acetate:*n*-hexane (3:7) as the eluent. The detailed characterization of 1,4-disubstituted 1,2,3-triazoles **5a**-**f** is given in the supplementary material.

Density functional theory (DFT) calculations

To find the electronic transitions and reaction conditions of the newly synthesized compounds, studies based on the DFT calculations were carried out. The optimization energy, polarizability, dipole moment, and all candidate compounds are given in Table 1 and Figure 2.

For all the optimized imidazole based 1,2,3-triazoles derivatives, the frontier molecular orbitals: such as the HOMO-LUMO orbitals and various global reactivity descriptors were calculated as shown in Table 1 and Figure 3. The energy needed to achieve a compound's most stable conformation is referred to as its optimization energy. According to the DFT findings, **5a** was found to have the lowest optimization energy and the most stable among all the synthesized compounds. The maximum optimization energy value in the series, however, is found in **5b**. In addition, **5b** exhibits a high degree of polarizability and a small dipole moment, as given in Table 1.

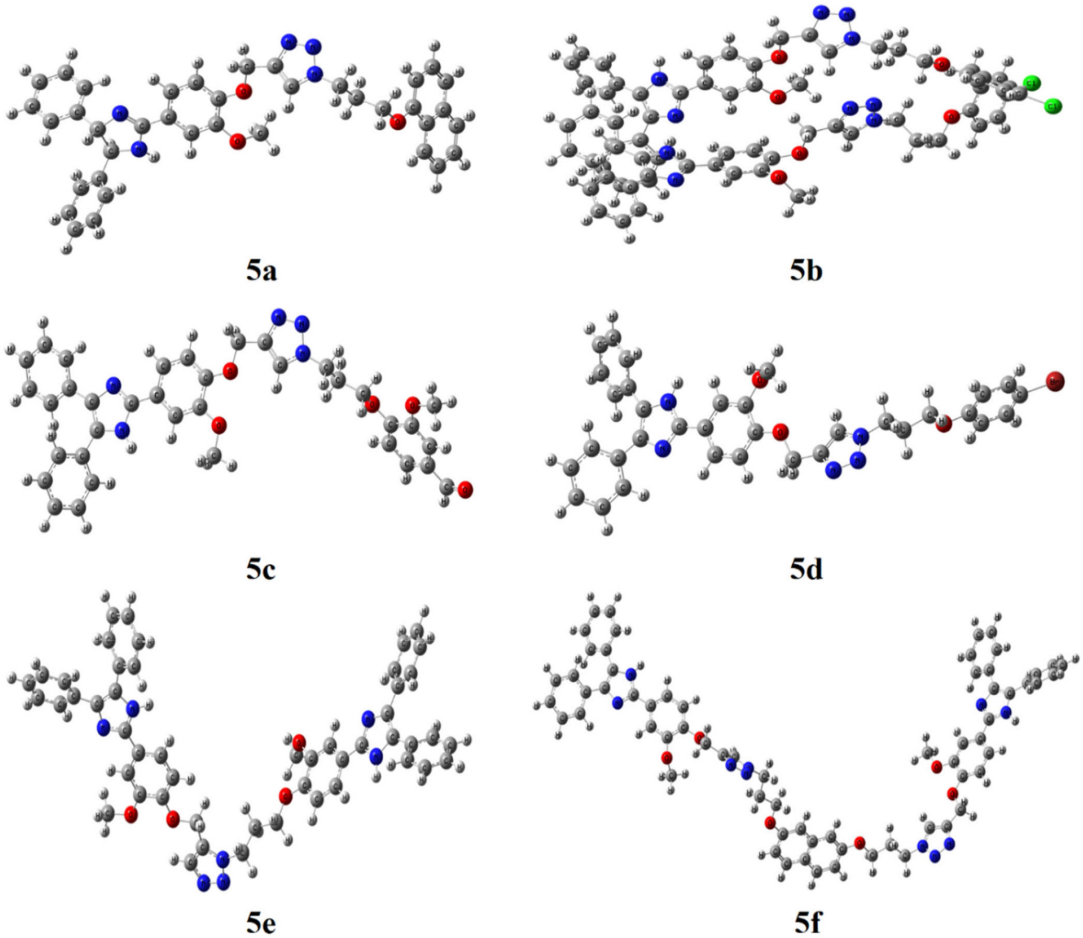

Figure 2. *The optimized structures of* ***5a-f*** *using B3LYP/6-31 G basis set*

Table 1. Calculations of optimization energies and FMOs of newly synthesized imidazole-based 1,2,3-triazoles

Codes	Optimization energy	Dipole moment	Polarizability (α)	HOMO (eV)	LUMO (eV)	HOMO-LUMO (eV)
5a	−1967.95	3.74	442.63	−0.21	−0.03	0.17
5b	−4583.60	7.33	872.27	−0.18	−0.05	0.14
5c	−2040.93	6.81	465.33	−0.19	−0.07	0.12
5d	−4384.13	5.04	444.28	−0.19	−0.04	0.15
5e	−2614.61	6.90	645.20	−0.19	−0.04	0.15
5f	−3547.74	9.64	856.42	−0.19	−0.04	0.15

HOMO: highest occupied molecular orbital. LUMO: lowest unoccupied molecular orbital.

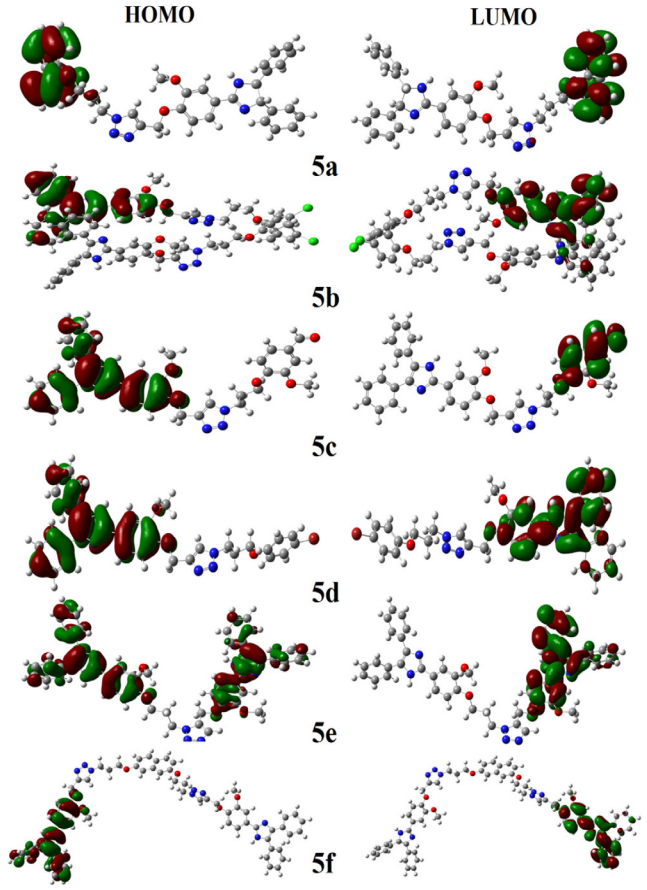

Figure 3. *HOMO-LUMO orbitals of newly synthesized imidazole-based 1,2,3-triazoles (**5a-f**)*

After careful analysis of the DFT calculations, it was found that compounds **5a** and **5d** have the most favourable energy gaps, indicating that they are the least reactive with Egap values of 0.173 and 0.153, respectively. Conversely, compound **5c** has the smallest energy gap with an Egap of 0.123, making it the most reactive. The HOMO energy values of **5a** and **5e** are the highest among all the compounds, with values of −0.206 and −0.193, respectively, while **5c** has the lowest LUMO energy of −0.0673. The compound possessing the maximum HOMO energy is regarded as the most effective electron donor, while the compound with the minimum LUMO energy is regarded as the most effective electron acceptor. Notably, the most potent compound, **5a**, has an energy gap of 0.172 and exhibits high stability. Among all the frontier molecular orbitals (FMO), the HOMO-LUMO orbitals are deemed the most significant in this quantum chemistry study. The accompanying Table 1 presents the values for all the parameters of the compounds.

The energy gap (LUMO-HOMO) of a molecule's HOMO and LUMO orbitals, known as the HOMO-LUMO band gap, can provide insight into its chemical reactivity. A larger HOMO-LUMO energy band gap suggests greater kinetic stability, less polarization, and a chemically hard compound with lower reactivity. Conversely, a smaller HOMO-LUMO energy band gap suggests a soft molecule with less stability, greater polarization, and higher reactivity. Figure 3 illustrates the HOMO-LUMO orbital energy values and other reactivity characteristics, such as chemical hardness and softness, for all compounds studied. The DFT data for each compound is relevant to their function. Compounds **5b** and **5c**, with low energy gap values, are expected to exhibit relatively high activity. The diagram displays the HOMO and LUMO orbitals, with derivatives possessing more stable LUMO orbitals anticipated to have greater biological activity. All derivatives possess a small chemical hardness, which shows that all are compounds with the same potential chemically. Table 2 is tabulated with local and global reactivity parameters of synthesized derivatives.

Carbonic anhydrase II inhibition assay

The inhibition potential of six novel compounds **5a-f** against CA II was evaluated using a modern version of an earlier described method.[18] As a reference, acetazolamide was used, and tris-sulfate buffer was used as a negative control. The IC_{50} values were determined by nonlinear regression using GraphPad Prism 5.0. The results showed that all six compounds exhibited potent inhibitory activity against CA II. Table 3 represents the inhibitory potential of newly synthesized imidazole-based 1,2,3-triazoles against CA.

Table 2. The reactivity profile of newly synthesized imidazole-based 1,2,3-triazoles (**5a-f**)

Codes	Chemical potential μ (eV)	Electronegativity X (eV)	Hardness η (eV)	Softness S (eV^{-1})	Electrophilicity index ω (eV)
5a	−0.12	0.12	0.09	5.80	0.08
5b	−0.12	0.12	0.07	7.37	0.10
5c	−0.13	0.13	0.06	8.15	0.14
5d	−0.12	0.12	0.08	6.57	0.09
5e	−0.12	0.12	0.08	6.58	0.09
5f	−0.12	0.12	0.07	6.73	0.09

Table 3. CA II inhibition values of newly synthesized imidazole-based 1,2,3-triazoles

Compound name	IC_{50} against CA II
3	2.691 ± 0.211
5a	0.032 ± 0.003
5b	0.076 ± 0.007
5c	0.069 ± 0.006
5d	0.084 ± 0.003
5e	0.063 ± 0.005
5f	0.025 ± 0.001
Acetazolamide[a]	0.96 ± 0.11[a]

[a]Acetazolamide (reference).

Structure-activity relationship

Structure-activity relationship (SAR) is a major tool used in drug discovery and development to understand how chemical modifications of a compound affect its biological activity. In the present study, six imidazole-based 1,2,3-triazoles; **5a**-**f** were synthesized and estimated for their inhibitory potential against the CA II enzyme. Among the synthesized compounds, **5f** exhibited the highest inhibitory activity against CA II (IC_{50} = 0.025 ± 0.001 μM) followed by **5a** (IC_{50} = 0.032 ± 0.003 μM), **5e** (IC_{50} = 0.063 ± 0.002 μM), **5c** (IC_{50} = 0.069 ± 0.006 μM), **5b** (IC_{50} = 0.076 ± 0.002 μM), and **5d** (IC_{50} = 0.084 ± 0.003 μM). The activity of compound **3** was also evaluated and it was observed that this exhibited the less inhibition as compared to all derivatives, suggesting the improved in inhibition potential of six imidazole-based 1,2,3-triazoles; **5a**-**f**.

A very interesting response was observed in the case of compounds **5a**, **5c**, and **5e**, which have a 4-(4,5-diphenyl-1*H*-imidazol-2-yl)-2-methoxyphenoxy)methyl substituent showed higher activity compared to the other compounds. This suggests that the imidazole ring plays an essential role in the inhibition of the CA II enzyme. Moreover, it can be observed that compounds **5a**, **5c**, and **5e** have a similar chemical structure except for the position of the methoxy group on the phenyl ring. The presence of the methoxy group at the *ortho* position in **5a** might be responsible for the higher inhibitory activity compared to the *meta* position in **5c** and *para* position in **5e**. This indicates that the position of substituents on the phenyl ring can also affect the activity of the compound.

On the other hand, when compared to the other compounds, those with a bisphenylmethane or naphthalene backbone, such as compounds **5b**, **5d**, and **5f**, displayed a lower level of activity. This suggests that the presence of a bulky substituent or a rigid backbone might make it more difficult for the compound to interact with the enzyme. All of the synthetic compounds exhibited higher inhibitory activity against CA II than the already-used effective acetazolamide. Because of this, it appears that the compounds based on imidazole and triazole moieties together in a single compound have the potential to be developed into new CA II inhibitors. In general, the results of the SAR analysis showed that the imidazole ring, the position of substituents on the phenyl ring, and the presence of a bulky or rigid backbone are important factors that affect the inhibition potential of the compounds against CA II. This information can be used in the future to guide the design and synthesis of CA II inhibitors that have a greater inhibitory effect.

Molecular docking studies

Molecular docking is widely used to determine the manner and extent of ligand-protein interactions. From the available docking programs, the AutoDock Vina is a popular choice due to its accuracy and user-friendly interface and is used in the current study. Molecular docking was performed to investigate the docking interactions of six different compounds **5a** to **5f** with bovine CA II. The investigation showed that compounds **5a** and **5f** exhibited the strongest inhibitory activity against CA II with the binding energy of −8.0 and −8.4 kcal mol^{-1}, respectively, surpassing the reference compound acetazolamide, a known CA II inhibitor, which exhibits −4.4 kcal mol^{-1} binding energy. These findings were consistent with the results of the carbonic anhydrase bioassay. Table 4 represents the molecular docking score of synthesized derivatives against CA II.

The docking results showed that the amino acid residues of an active pocket of CA II LEU237 formed pi-sigma while the rest of the amino acid residues of the active pocket *i.e.* PHE229 and HIS A: 2 π-π stacked and π-π T shaped respectively with **5a** compound as shown in Figure 4.

Table 4. Docking energy values of acetazolamide and all the triazole derivatives

Compound	Docking score (kcal mol^{-1})
5a	−8.0
5b	−4.6
5c	−6.8
5d	−7.5
5e	−6.3
5f	−8.4
Acetazolamide	−4.4

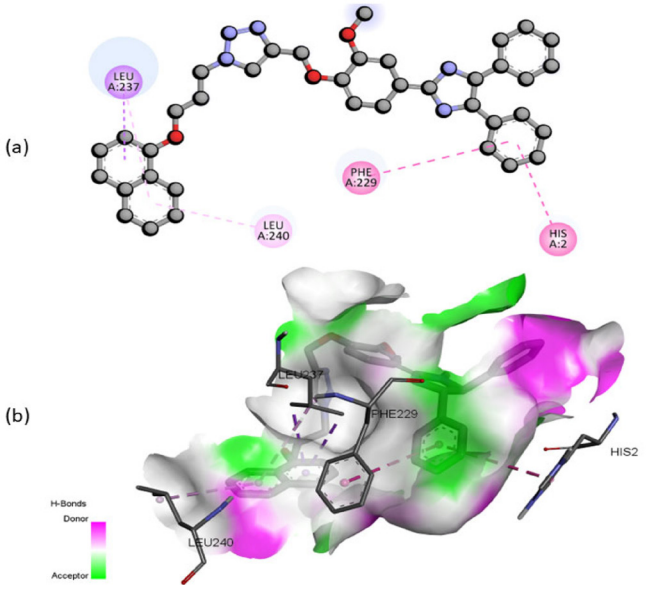

Figure 4. *The 2D (a) and 3D (b) binding mode of compound* ***5a*** *within the active pocket of CA II*

The 2D and 3D binding interactions of the **5f** derivative with the active pocket of the target protein were analyzed, revealing that specific amino acid residues played key roles in the binding interactions of each compound as shown in Figure 5. For **5f**, GLN219, GLN 156, LYS223, LEU159, ALA151, PRO153, and LYS157 were found to be the primary amino acid residues involved in different types of interactions. Among these interactions, it was observed that no hydrogen bond was formed between the benzene ring of **5f**

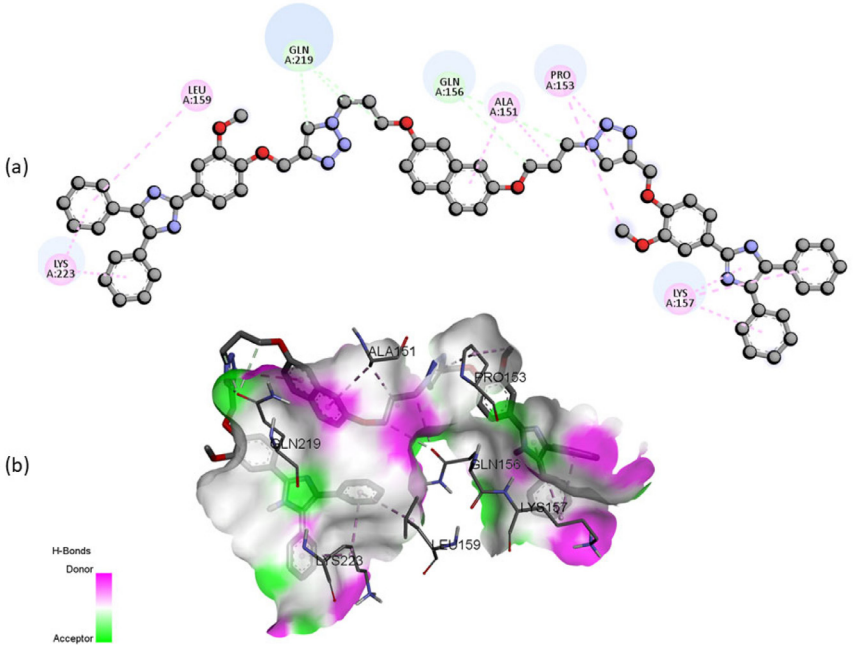

Figure 5. *The predicted 2D (a) and 3D (b) binding mode of compound* ***5f*** *within the active pocket of CA II*

and protein residues, while other amino acid residues GLN219 and GLN156 contributed to carbon-hydrogen bond interactions. Amino acid residues LYS223, LEU159, ALA151, PRO153, and LYS157 were found to have alkyl and π-alkyl interactions.

In contrast, the docking interactions of acetazolamide as shown in Figure 6 involved three strong hydrogen bonds formed by the ASP160, SER164, and LYS157, with π-sigma interaction observed with only ALA161 amino acid residue within the active pocket of CAII.

Overall, these results indicate that compounds **5a** and **5f** have potent inhibitory potential against CA II and suggest specific amino acid residues involved in the binding interactions of these compounds. The findings from this study may be useful in the development of new CA II inhibitors. Docking results of other compounds are given in Figure 13S-16S (supplementary material).

Molecular dynamic simulations

The visual molecular dynamics (VMD) interface was utilized to predict and visualize the trajectories of molecular dynamics based on numerically integrated mathematical equations. Structural properties were analyzed using root mean square deviation (RMSD), root mean square fluctuations (RMSF), hydrogen bonds analysis, solvent accessible surface area (SASA), and radius of gyration calculations. This article boons the outcomes obtained from this analysis, describing an insightful view regarding the stability and mechanical transitions of molecules.

RMSD analysis revealed the structural stability of the molecules under consideration. Ligand-protein complex possessed notable conformational stability with an average value of 3.20 Å as shown in Figure 7a. The apoprotein molecule exhibited the highest stability under the provided conditions, as evidenced by an average RMSD value of 1.38 Å while the ligand **5f** molecule average RMSD of ligand 7.15 Å revealed that, respectively. RMSD values suggested that the system remained well-equilibrated throughout the simulation time. These differences in the RMSD values can be accredited to the presence of additional molecular interactions in the ligand-protein complex, exhibiting substantial molecular rearrangements in the system. To further evaluate the dynamics of the molecules, root mean square fluctuations (RMSF) were calculated. The RMSF values provide insights into the flexibility and stability of individual atoms or groups within a biomolecular system. Analysis of the RMSF profiles revealed distinct peaks and valleys, indicating regions of local conformational changes. Lower RMSF values suggest that the atoms or groups are relatively stable and exhibit less fluctuation. These observations suggest that the molecular rearrangements were restrained and stable throughout the simulation time, with little fluctuations at the beginning and end. The RMSF average value of 0.72 Å suggests that amino acid residues are stable and exhibit low

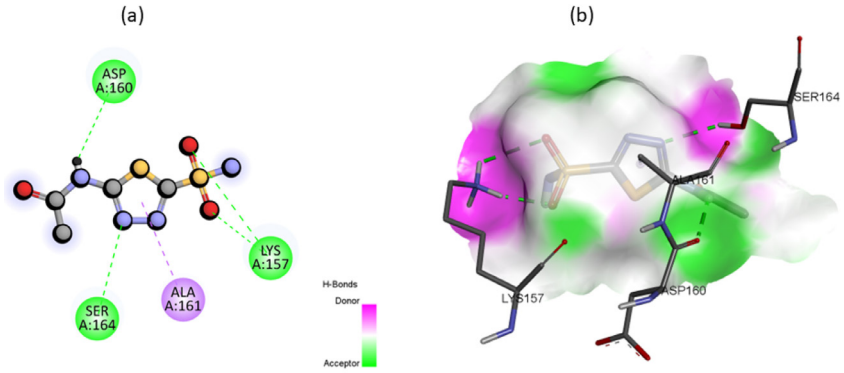

Figure 6. *The predicted 2D (a) and 3D (b) binding mode of reference compound acetazolamide within the active pocket of CA II*

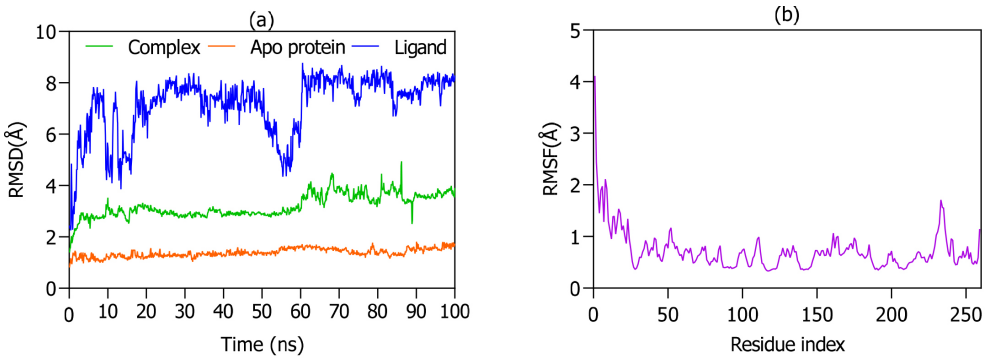

Figure 7. *(a) Root mean square deviation (RMSD) plot showing the structural stability of ligand* ***5f****, apoprotein (CA II), and the* ***5f****-CAII complex. (b) Root mean square fluctuations (RMSF) plot exhibiting the flexibility of apoprotein (CA II)*

flexibility which supports the potent ligand protein interactions as shown in Figure 7b.

Electrostatic interactions among the ligand **5f** and protein (CA II) can be analyzed by evaluating the amino acid residues forming hydrogen bonds with the ligand molecules. From Table 5, the analysis highlights that SER217, GLN156, GLN219, LYS223 and LYS157 amino acid residues of CA II have strong potential to develop hydrogen bond network with ligand **5f** side atoms leading towards more stable protein-ligand complex as shown in Figure 8.

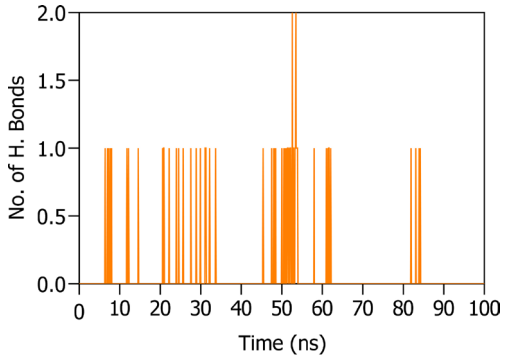

Figure 8. *The plot of distribution of hydrogen bonds between ligand* ***5f*** *and CA II*

This distribution provides insights into the dynamic behavior of hydrogen bonds, highlighting the varying levels of bond formation and breakage throughout the simulation trajectory. Understanding the fluctuation in hydrogen bond numbers aids in characterizing the stability and interactions within the molecular system.

Furthermore, solvent accessible surface area (SASA) analysis revealed that various regions of an apoprotein exhibit different exposure to solvent molecules. Peaks in Figure 9a revealed that protein

Table 5. Results of hydrogen bond interactions during MD simulations

Serial No.	Donor	Acceptor
1	SER217-Side	**5f**-side
2	GLN219-side	**5f**-side
3	GLN156-side	**5f**-side
4	LYS223-side	**5f**-side
5	**5f**-side	GLN219-side
6	LYS157-side	**5f**-side
7	**5f**-side	ALA151-main

regions were more exposed to the solvent as the conformational changes progressed while valleys suggest the buried residues were tightly packed and had limited solvent exposure, respectively. These regions often contribute to the overall stability and folding of the biomolecules. Radius of gyration (Rg) based interpretations indicate the average distance between the atoms in a biomolecule and its centre of mass. In the current analysis, the Rg plot revealed trough regions in Figure 9b showing the compactness of the globular conformation of the apoprotein molecule possessing well-folded and intact residues of apoprotein while crest regions indicating the distorted conformation having flexible regions of the molecule.

ADMET analysis

The synthesized derivatives **5a** and **5f** underwent evaluation for their physicochemical properties using the ADMET predictor. The analysis showed that compounds **5a** and **5f** depict less GI absorption with logP value 4.629 and 4.648, respectively, demonstrating the compounds have a preference for hydrophobic environment. The comprehensive physicochemical and pharmacokinetic profiles of these derivatives are described in Table 6.

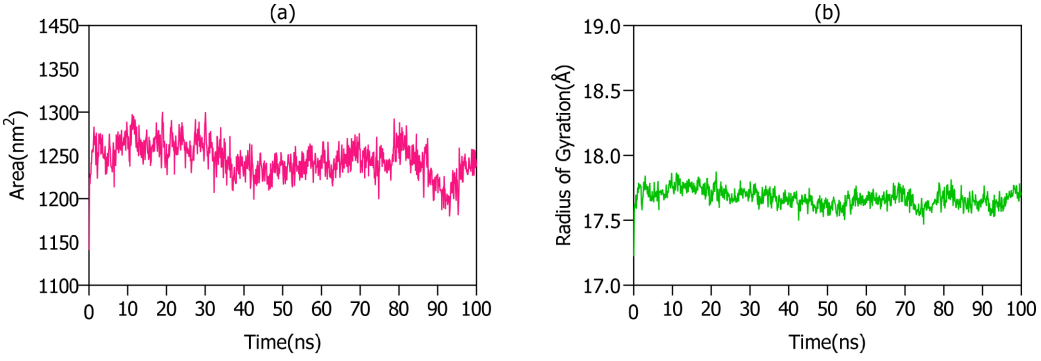

Figure 9. *(a) Solvent accessible surface area (SASA) plot depicting the solvent accessible surface area of CA II during the molecular dynamics simulation. (b) The radius of gyration indicates the compactness of CA II*

Table 6. Physicochemical and pharmacokinetic properties of compounds **5a** and **5f**

Parameters	**5a**	**5f**
Diff. coef.	0.496	0.352
M. logP	4.629	4.648
S + logP	7.015	9.364
S + logD	4.761	9.057
Rule of 5	2	3
Rule of 5_Code	Mw; LP	Mw; LP
Mw	609.732	1095.322
nHA	8	16
T_PSA	82.79	164.92
nHD	1	4

Diff. coef.: Differential coefficient. nHA: Number of hydrogen bond acceptor. T_PSA: Topological polar surface area. nHD: Number of hydrogen donor. Mw: Molecular weight. LP: Lipophilicity.

CONCLUSIONS

A series of imidazole-based 1,2,3-triazoles derivatives were synthesized and analyzed as carbonic anhydrase II inhibitors. Among the derivatives, compounds **5f** and **5a** exhibited the most promising inhibitory potential, with IC_{50} values of 0.025 ± 0.001 and 0.032 ± 0.003 μM, respectively. Both **5a** and **5f** derivatives have comparable inhibitory potential but **5f** was found to be more potent than **5a**. To investigate the electronic properties and different reactivity parameters of all synthesized compounds, the DFT calculations were carried out. The binding modes of every compound with CA II were also investigated using molecular docking. The docking results revealed that all compounds interacted favorably with the active pocket of the CA II enzyme. Compounds **5f** and **5a** exhibited the highest binding affinity, which corresponds to its potent inhibitory activity. Compound **5f** exhibited the most potent CA II inhibiting activity, and DFT and molecular docking studies revealed its electronic properties and binding interactions with the enzyme. Furthermore, molecular dynamic simulation studies highlight the most significant conclusion that compound **5f** develops stable interaction with the active pocket of CA II. By comparing the MD simulation results with experimental data, we confirmed the accuracy and reliability of our computational approach, further validating the significance of hydrogen bonds in the studied system. Although limitations in the simulation methodology exist, careful consideration of these factors was undertaken to ensure the validity of the results. Compound **5f** has the potential to be further optimized as a therapeutic agent for CA II-related diseases. These findings contribute significantly to the existing knowledge, paving the way for the future development of potent and novel inhibitors against carbonic anhydrase II.

SUPPLEMENTARY MATERIAL

Supplementary information contains the NMR spectra of the synthesized compounds and is available at http://quimicanova.sbq.org.br/, as a PDF file, with free access.

ACKNOWLEDGMENTS

This research was funded by Princess Nourah Bint Abdulrahman, Univeristy Researchers supporting project number (PNURSP2024R116), Princess Nourah Bint Abdulrahman University, Riyadh, Saudi Arabia.

The authors declare no conflict of interest.

REFERENCES

1. Hussain, T.; Ullah, S.; Alrokayan, S.; Alamery, S.; Mohammed, A. A.; Ejaz, S. A.; Aziz, M.; Iqbal, J.; *RSC Adv.* **2023**, *13*, 18461. [Crossref]
2. Al-Rashida, M.; Ejaz, S. A.; Ali, S.; Shaukat, A.; Hamayoun, M.; Ahmed, M.; Iqbal, J.; *Bioorg. Med. Chem.* **2015**, *15*, 2435. [Crossref]
3. Er, A.; *Lett. Drug Des. Discovery* **2023**, *20*, 1427. [Crossref]
4. Capasso, C.; *Int. J. Mol. Sci.* **2023**, *10*, 7014. [Crossref]
5. Lee, S. K.; Boron, W. F.; Occhipinti, R.; *Int. J. Mol. Sci*. **2023**, *24*, 4251. [Crossref]
6. Rulhania, S.; Kumar, S.; Nehra, B.; Gupta, G. D.; Monga, V.; *J. Mol. Struct.* **2021**, *15*, 129982. [Crossref]
7. Wu, X.; Wang, J.; Xia, S.; Cheng, S.; Shi, Y.; *Curr. Top. Med. Chem.* **2022**, *22*, 1406. [Crossref]
8. Nepali, K.; Lee, H. Y.; Liou, J. P.; *J. Med. Chem.* **2018**, *62*, 2851. [Crossref]
9. Ali, E. S.; Chakrabarty, B.; Ramproshad, S.; Mondal, B.; Kundu, N.; Sarkar, C.; Sharifi-Rad, J.; Calina, D.; Cho, W. C.; *Cell Commun. Signaling* **2023**, *21*, 145. [Crossref]
10. Lee, J. S.; Hackbart, H.; Cui, X.; Yuan, Y.; *Int. J. Mol. Sci.* **2023**, *24*, 11791. [Crossref]
11. Bonandi, E.; Christodoulou, M. S.; Fumagalli, G.; Perdicchia, D.; Rastelli, G.; Passarella, D.; *Drug Discovery Today* **2017**, *22*, 1572. [Crossref]
12. Dheer, D.; Singh, V.; Shankar, R.; *Bioorg. Chem.* **2017**, *71*, 30. [Crossref]
13. Abdelli, A.; Azzouni, S.; Plais, R.; Gaucher, A.; Efrit, M. L.; Prim, D.; *Tetrahedron Lett.* **2021**, *86*, 153518. [Crossref]
14. Ruzi, Z.; Nie, L.; Bozorov, K.; Zhao, J.; Aisa, H. A.; *Arch. Pharm.* **2021**, *354*, 2000470. [Crossref]
15. Shalmali, N.; Ali, M. R.; Bawa, S.; *Mini-Rev. Med. Chem.* **2018**, *18*, 142. [Crossref]
16. Al-Adilee K. J.; Jawad S. H.; Kyhoiesh, H. A.; Hassan, H. M.; *J. Mol. Struct.* **2024**, *1295*, 136695. [Crossref]
17. Kumar, C. P.; Prathibha, B. S.; Prasad, K. N.; Raghu, M. S.; Prashanth, M. K.; Jayanna, B. K.; Alharthi, F. A.; Chandrasekhar, S.; Revanasiddappa, H. D.; Kumar, K. Y.; *Bioorg. Med. Chem. Lett.* **2021**, *36*, 127810. [Crossref]
18. Ana, G.; Kelly, P. M.; Malebari, A. M.; Noorani, S.; Nathwani, S. M.; Twamley, B.; Fayne, D.; O'Boyle, N. M.; Zisterer, D. M.; Pimentel, E. F.; Endringer, D. C.; *Pharmaceuticals* **2021**, *14*, 169. [Crossref]
19. Penthala, N. R.; Madhukuri, L.; Thakkar, S.; Madadi, N. R.; Lamture, G.; Eoff R, L.; Crooks, P. A.; *MedChemComm* **2015**, *6*, 1535. [Crossref]
20. Fanelli, S.; Zimmermann, A.; Totoli, E. G.; Salgado, H. R.; *J. Chem.* **2018**, *2018*, 1. [Crossref]
21. Tampieri, A.; Szabó, M.; Medina, F.; Gulyás, H.; *Physical Sciences Reviews* **2020**, *6*, 20190086. [Crossref]
22. Neiss, T. G. In *Encyclopedia of Analytical Chemistry: Applications, Theory, and Instrumentation*; Meyers, R. A. ed.; John Wiley & Sons: Hoboken, 2006. [Crossref]
23. Kaufmann, A.; Walker, S.; *Rapid Commun. Mass Spectrom.* **2018**, *30*, 503. [Crossref]
24. Frisch, M. J.; Trucks, G. W.; Schlegel, H. B.; Scuseria, G. E.; Robb, M. A.; Cheeseman, J. R.; Scalmani, V.; Barone, G.; Petersson, G. A.; Nakatsuji, H.; *Gaussian 09*; Gaussian Inc.; Wallingford, CT, USA, 2009.
25. Beck, A. D.; *J. Chem. Phys.* **1993**, *98*, 5648. [Crossref]
26. Todd, R. D.; Keith, A.; Millam, J. M.; *GaussView*, version 6; Semichem Inc.; Shawnee Mission, KS, USA, 2016.
27. Bendjeddou, A.; Abbaz, T.; Gouasmia, A.; Villemin, D.; *Am. J. Appl. Chem.* **2016**, *4*, 104. [Crossref]

28. Ejaz, S. A.; Farid, A.; Zargar, S.; Channar, P. A.; Aziz, M.; Wani, T. A.; Attaullah, H. M.; Ujhan, R.; Tehzeeb, A.; Saeed, A.; Ali, H. S.; *BMC Chem.* **2023**, *17*, 97. [Crossref]
29. Saeed, A.; Ejaz, S. A.; Ul-Hamid, A.; El-Seedi, H. R.; Iqbal, J.; *J. Mol. Struct*. **2021**, *1243*, 130821. [Crossref]
30. Saeed, A.; Ejaz, S. A.; Saeed, M.; Channar, P. A.; Aziz, M.; Fayyaz, A.; Zargar, S.; Wani, T. A.; Alanazi, H.; Alharbi, M.; Iqbal, J.; *Polycyclic Aromat. Compd.* **2023**, *10*, 1. [Crossref]
31. Burley, S. K.; Berman, H. M.; Kleywegt, G. J.; Markley, J. L.; Nakamura, H.; Velankar, S.; *Methods Mol. Biol.* **2017**, *1607*, 627. [Crossref]
32. Saito, R.; Sato, T.; Ikai, A.; Tanaka, N.; *Acta Crystallogr., Sect. D: Biol. Crystallogr.* **2004**, *60*, 792. [Crossref]
33. McKinnon, J. J.; Jayatilaka, D.; Spackman, M. A.; *Chem. Commun.* **2007**, *33*, 3814. [Crossref]
34. Brown, T.; *The Science Teacher* **2014**, *81*, 67. [Crossref]
35. Li, Y.; Han, L.; Liu, Z.; Wang, R.; *J. Chem. Inf. Model.* **2014**, *54*, 1717. [Crossref]
36. Barclay, P. L.; Zhang, D. Z.; *J. Comput. Phys.* **2021**, *435*, 110238. [Crossref]
37. Bowers, K. J.; Chow, E.; Xu, H.; Dror, R. O.; Eastwood, M. P.; Gregersen, B. A.; Klepeis, J. L.; Kolossvary, I.; Moraes, M. A.; Sacerdoti, F. D.; Salmon, J. K.; *Proceedings of the 2006 ACM/IEEE Conference on Supercomputing*; Tampa, Florida, 2006. [Crossref]
38. Martyna, G. J.; Tobias, D. J.; Klein, M. L.; *J. Chem. Phys*. **1994**, *101*, 4177. [Crossref]
39. Luty, B. A.; *Mol. Simul.* **1994**, *14*, 11. [Crossref]
40. Humphreys, D. D.; Friesner, R. A.; Berne, B. J.; *J. Phys. Chem. A* **1994**, *98*, 6885. [Crossref]
41. Hassan, S. F.; Rashid, U.; Ansari, F. L.; Ul-Haq, Z.; *J. Mol. Graphics Modell.* **2013**, *45*, 202. [Crossref]